Measurement 139 (2019) 185–195

Contents lists available at ScienceDirect

Measurement

journal homepage: www.elsevier.com/locate/measurement

Width measurement for pathological vessels in retinal images using centerline correction and *k*-means clustering

Gang Sun [a], Xiaoyan Liu [a,b,*], Siyuan Wang [a], Ling Gao [c], Min Liu [a]

[a] College of Electrical & Information Engineering, Hunan University, Changsha 410082, China
[b] Hunan Key Laboratory of Intelligent Robot Technology in Electronic Manufacturing, Changsha 410082, China
[c] Central South University, The Second Xiangya Hospital, Department of Ophthalmology, Changsha 410011, China

ARTICLE INFO

Article history:
Received 11 October 2018
Received in revised form 28 January 2019
Accepted 3 March 2019
Available online 4 March 2019

Keywords:
Retinal image
Vessel width
K-means
Image segmentation

ABSTRACT

Changes in retinal blood vessel width and morphology are closely related to the development of many diseases. However, some vessels (especially pathological vessels) often show central light reflex in retinal images, making it difficult to detect the vessel boundary and to measure the vessel width. In this study, a measuring methodology is proposed to improve the performance in measuring blood vessels with central light reflex, by use of centerline correction and *k*-means clustering algorithm. Firstly, the vessel tree in the retinal image is segmented using Isotropic Undecimated Wavelet Transform. Then, the centerline of each vessel is roughly extracted using morphological thinning algorithm, and corrected for vessels with central light reflex by use of a parallel line model. With known centerline, the direction and length of the measuring axis are determined, and the intensity profile of the pixels along the axis is obtained. By use of *k*-means clustering algorithm for the intensities, the pixels on the measuring axis are classified into vessel and background, based on which the vessel width is finally determined. The proposed method is tested on the public dataset REVIEW and our own dataset, and compared with ground truth and state-of-the-art method (ARIA method). It is shown that the measuring accuracy of proposed method is comparable to ARIA (average relative error: 3% vs. 4%), but it is more advantageous in measuring pathological vessels with central light reflex. It succeeds in measuring all the testing pathological vessels whereas ARIA is capable of measuring 20% of them. Result of the work has potential usage in quantitative evaluation of the progressing of retinal diseases.

1. Introduction

Retinal imaging is a non-invasive technique to photograph retinal vasculature in vivo, and has been widely used for the diagnosis of many ocular diseases [1–3]. In the analysis of retinal image, the vessel width is usually examined: small variations in vessel width is a normal phenomenon caused by autonomic regulation of blood flow [4], while sustained change in vessel width may be related with retinopathy or diseases in circulatory system such as coronary heart disease, diabetes and hypertension [5,6]. For objective evaluation and diagnosis, the measurement of the vessel width should be quantitative and accurate [7–9].

Some commercial software are available for measurement of the distance between pixels in an image, such as Image-Pro® that has been widely used for medical image analysis [10]. However, when measuring the vessel width, the user has to manually determine both the cross section and the boundary of the vessel, which may lead to subjective results with bad reproducibility, as was pointed out in [11]. To solve this problem, great efforts [12–20] have been made to develop methods for automatic measurement of vessel width in retinal images. These methods generally consist of four main steps: (i) extraction of the vessel tree using a certain image segmentation algorithm, such as wavelet transformation [20], matched filters [14,15] or thresholding [13,18]; (ii) extraction of the vessel centerline using morphological thinning algorithm [13,15,18] or tramline algorithm [17]; (iii) approximation of the cross section intensity profile of the vessel with Gaussian model [14–16], or multi-resolution Hermite model [19], ROT active contour model [17] or two-slice 3-D surface model [18]; (iv) detection of the vessel boundary based on cross section intensity profile of the vessel by using two pairs of contours [17], or ensembles of bagged decision trees [19], or by locating the inflection point [15,20].

* Corresponding author at: College of Electrical & Information Engineering, Hunan University, Changsha 410082, China.
E-mail address: xiaoyan.liu@hnu.edu.cn (X. Liu).

https://doi.org/10.1016/j.measurement.2019.03.005
0263-2241/

The main challenge in measuring vessel width in retinal images lies in the measurement of pathological vessels with central light reflex (see Fig. 1(a)), where the shape and smoothness of intensity profiles [21] of the vessel is distorted. The central light reflex is generated from a rough reflecting surface and the intravascular erythrocytes [22], and appears to be associated with diseases like hypertension and arteriosclerosis [23,24]. In malignant cases, the central light reflex may even start touching the vessel borderlines and the intensity of vessel centerline is completely deteriorated. This abnormality is known as 'arteriosclerosis' and the extreme stages are referred as 'copper-wiring' and 'silver-wiring' [25]. Some methods are available in literature to measure vessels with central light reflex. Lowell et al. [15] employed a double Gaussian model to fit the combined profiles of vessels and light reflex. The fit of the model is good when pixels at two sides of the vessels are homogenous in intensity. However, vessel width is likely incorrectly measured when the background pixels significantly differ from each other. Al-Diri et al. [17] presented a ESP method for measuring retinal vessels by a parametric active contour. The algorithm is generally good in obtaining various vessel edges. The incorrect measuring happens most in the measurement of closely parallel vessels [17]. Xu et al. [18] employed graph-based algorithm to search the vessel edges by first computing intensity profiles across vessel centerlines and then determining the edges from the profiles by minimizing a cost function. The method shows satisfied performance except on the vessels near crossing and branching points of vessels. Bankhead et al. [20] compared the performance of different measuring methods for the vessel width, including 2D Gaussian [15], ESP [17], graph-based method [18], the HHFW method [12], 1D Gaussian [14], and the method using wavelets and edge location refinement (ARIA method) [20]. Comparative study in [20] demonstrates that, the most recent three methods (ESP method, graph-based method and ARIA method) outperform other methods in measuring accuracy, and ARIA shows better performance in measuring vessels with central light reflex in REVIEW dataset [26]. Therefore, ARIA can be taken as state-of-the-art technique in measuring vessel width. Nevertheless, for pathological vessels with relatively stronger central light reflex (as shown in Fig. 1 for example), ARIA method may fail because the vessel is incorrectly recognized as two separated vessels with different centerlines.

Inspired by these recent studies and the increasing needs in measuring pathological vessels, we propose an improved methodology for automatic vessel width measurement. It is based on ARIA method but has improvement in centerline extraction and boundary detection of pathological vessels, by use of a parallel line model and *k*-means clustering algorithm.

The proposed measuring method is described in detail in Section 2. The effectiveness of the proposed method is tested in Section 3, using the public REVIEW database [26] and our own dataset which contains more pathological vessels. The vessel width measured by the proposed method is then compared with that by the state-of-the-art method (ARIA method) and ground truth. The results are discussed in Section 4, with main conclusions summarized in Section 5.

2. Methods

The proposed workflow for measuring vessel width in retinal image is illustrated in Fig. 2. It consists of following main procedures: (i) segmentation of blood vessels by Isotropic Undecimated Wavelet Transform (IUWT); (ii) extraction and refinement of centerlines by use of morphological thinning algorithm, parallel line model correction and cubic spline fitting; (iii) generation of the measuring axis based on refined centerline; (iv) identifying vessel boundaries by *k*-means clustering and boundary searching strategy; and (v) calculation of the vessel width. It is noted that steps in procedure (ii) are necessary for generating refined centerlines: the employ of morphological thinning algorithm is for obtaining rough centerlines of segmented vessels; the usage of parallel line model is to correct possible wrong centerlines; and the step cubic spline fitting of rough centerlines is to refine centerlines. With the refined centerlines, measuring axis can be generated and vessel width can be calculated. In the following sections, each procedure will be described in detail.

2.1. Vessel segmentation by IUWT method

For automatic measurement of the vessel width, the vessel tree (see Fig. 3(a)) in retinal images should be extracted first. In the present work, the green channel of the color retinal image is used because it has best contrast, as was also done in [27]. It should be pointed out that the present work and ARIA method employed the same method of IUWT [28] for vessel segmentation because IUWT has many features that are suitable for our application: it is translation invariant, redundant, and particularly simple and fast to implement. In the segmentation procedure by IUWT method, a grey retinal image is firstly reconstructed as a image with wavelet

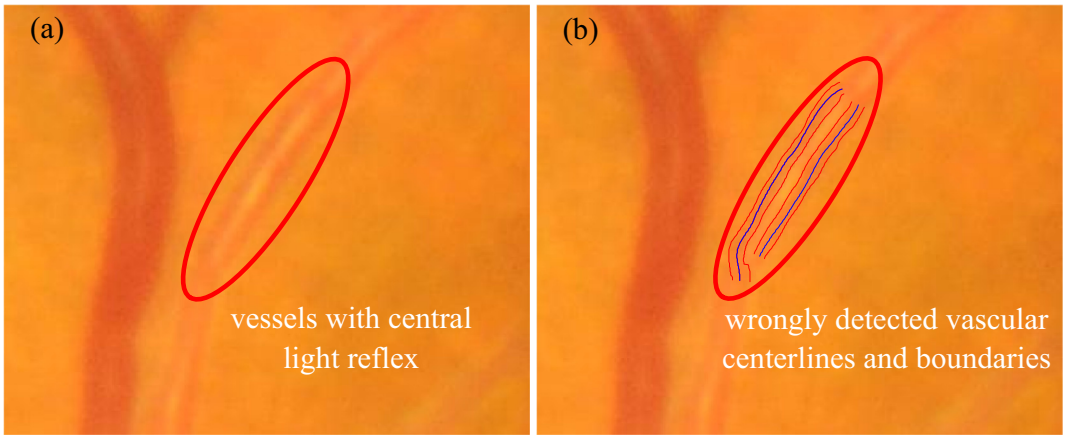

Fig. 1. Example of vessels with arteriosclerosis: (a) a vessel segment with strong central light reflex; (b) wrongly extracted centerlines (blue colored) and vessel boundaries (red colored) by ARIA method. (For interpretation of the references to colour in this figure legend, the reader is referred to the web version of this article.)

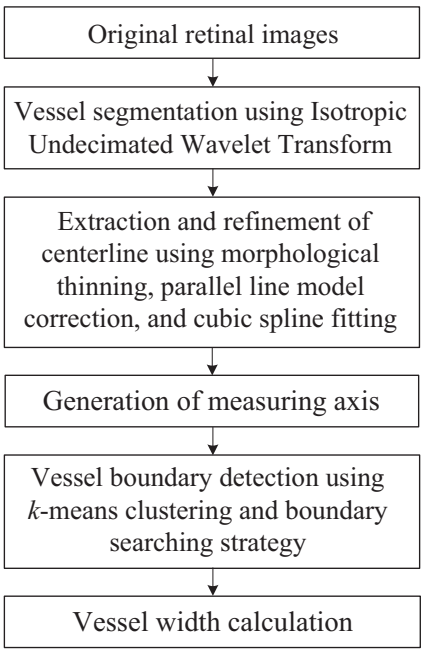

Fig. 2. Workflow of the proposed measuring methodology.

coefficients; then a percentage of pixels with the lowest wavelet coefficients within the view field are selected as blood vessels; finally, segmentation result is improved by removing small isolated objects.

To reconstruct original image as image with wavelet coefficients, in IUWT, the scaling coefficients, which retain the mean of original signal, are firstly obtained by low-pass filtering. Denote the scaling coefficient at iteration j as c_j, the value at iteration $(j+1)$ is the convolution of

$$c_{j+1} = c_j * h^{\uparrow j} \tag{1}$$

where $h^{\uparrow j}$ is the augmented filter obtained by inserting $(2^j - 1)$ zeros between each pair of adjacent coefficients of h_0 derived from the cubic B-spline

$$h_0 = [1, 4, 6, 4, 1]/16 \tag{2}$$

For iteration, the initial scaling coefficient c_0 is set to the gray matrix of the original image I. With known scaling coefficients, the wavelet coefficients w_j, which encode the information corresponding to different spatial scales present within the signal, can be then obtained by

$$w_{j+1} = c_j - c_{j+1} \tag{3}$$

After the computation of n wavelet levels, the original image can be finally reconstructed as

$$I = c_n + \sum_{j=1}^{n} w_j \tag{4}$$

After the reconstruction procedure, wavelet coefficients of blood vessels should be identified. Blood vessels in retinal images are generally darker than background and thus have low wavelet coefficients. For this reason, segmented vessels (shown in Fig. 3 (b)) can be obtained by retaining a percentage of pixels with the lowest coefficients from the best contrast reconstruction image. Typically, the proportion of vessel pixels within the view field is around 12–14% [20]. The wavelet levels and thresholds could vary according to different image sizes, but basically remain unchanged for images of similar size. In the present work, we set the threshold to recognize the lowest 20% of wavelet coefficients within the view field as vessels in all circumstances, and the wavelet levels are changed corresponding to different image sizes.

After thresholding the image with wavelet coefficients, there maybe some background pixels which are misidentified as vessels. Most of these misidentified vessels are small and isolated. These isolated non-vessel parts are finally removed from the extracted vessel structure by use of connected components labeling method, with improved segmentation results shown in Fig. 3(c).

2.2. Centerline extraction and refinement

The extraction and refinement of centerline is important for determining vessel directions. In the present work, the centerline of each vessel is roughly extracted by morphological thinning algorithm, with the following step of parallel line model correction and cubic spline fitting.

The morphological thinning algorithm described in [20] is employed to obtain a rough centerline map, in which shifting and logical operations with structural elements are performed continuously to segmented vessels until only vessel centerlines are remained. The 8-connected components of pixels within the rough centerline map are then labeled. After this procedure, centerlines of vessel segments can be separated from rough centerline map by deleting joint pixels (having more than 2 adjacent pixels) at branching and crossing points.

With the method described above, the centerline of most vessels can be correctly extracted, as shown in Fig. 4(a). However, the method fails for some pathological vessels that have central light reflex. These vessels are incorrectly treated as two separated vessels with two centerlines, as shown in Fig. 4(c) for example.

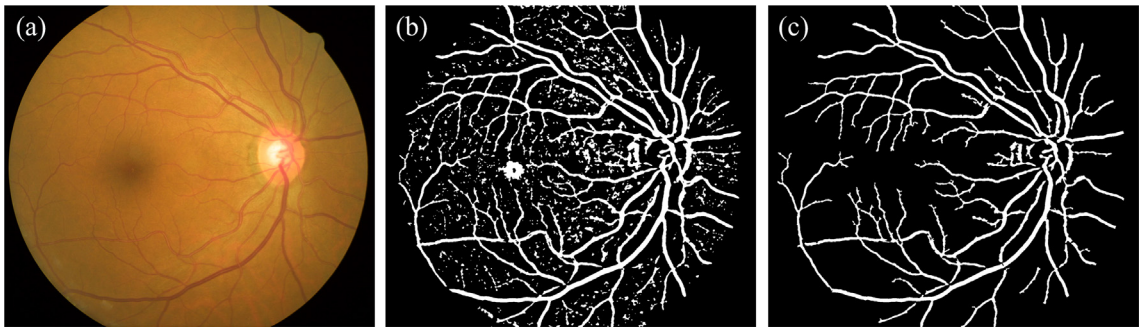

Fig. 3. Example of blood vessel segmentation: (a) a retinal image from the REVIEW database; (b) segmentation result after thresholding; (c) improved segmentation result after removing small sized objects.

Therefore, it is necessary to develop a new method to detect and correct centerlines of vessels with central light reflex.

When observing the two wrong centerlines shown in Fig. 4(c), we can find that they are approximately parallel and very close to each other. Based on these features, we propose a parallel line model (Fig. 5) to detect and correct these wrong centerlines. In Fig. 5, L1 and L2 are the supposed parallel centerlines with points $A_i(i = 1, 2, \ldots, n)$ and $B_i(i = 1, 2, \ldots, n)$, $[O_1, \cdots O_i, \cdots, O_n]$ are the points in between. For each centerline segment L_1, it will be identified as wrong centerline if there exists another centerline segment L_2 satisfying the condition that for all the points A_i in L_1, the shortest Euclidean distance $A_iB_i(i = 1, 2, \cdots, n)$ between the point A_i and L_2 are approximately equal to a constant a. In the detection of point pairs A_i, B_i from the two lines, a brute force search is employed in the present work. With this method, the two wrong parallel centerlines L_1 and L_2 (Fig. 4(d)) of the vessel with light reflex can be detected. The corresponding rough centerline is then corrected as the pixels $([O_1, \cdots O_i, \cdots, O_n])$ with averaged coordinates of $A_i, B_i(i = 1, 2, \ldots, n)$, as shown in Fig. 4(e) for example. Pairs of centerline segments at the branching or crossing part of vessels may have similar direction and tend to be misidentified as parallel. These spurious centerline pairs are usually short (less than 10 pixels) and are excluded before the step of parallel-line-model correction.

With corrected rough centerlines by use of parallel line model, the direction of vessel centerlines should be calculated. The resolutions of angles estimated from centerlines with discrete pixels are somewhat low. In order to solve this problem, the centerlines are fitted into refined centerlines by least-squares cubic spline.

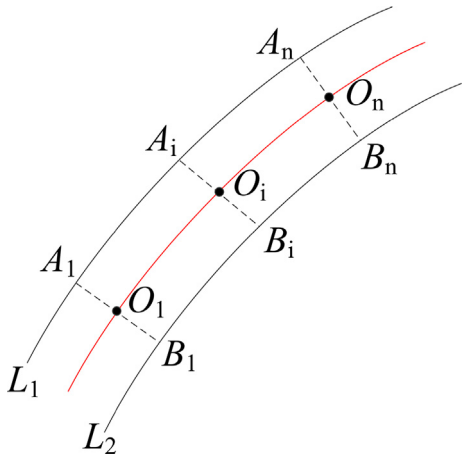

Fig. 5. Illustration of the parallel line model.

2.3. Generation of the measuring axis

After the procedure of centerline extraction and refinement, the measuring axis should be generated. With the refined centerlines obtained in Section 2.2, the vessel direction (derivative) at any point of the centerlines becomes calculable, measuring axis which is perpendicular to the vessel direction is then easily obtained. The raw intensity data of the image are linearly interpolated, and the intensity profiles of vessel pixels along the measuring axis are then selected. Fig. 6 shows for example the generated axis and the

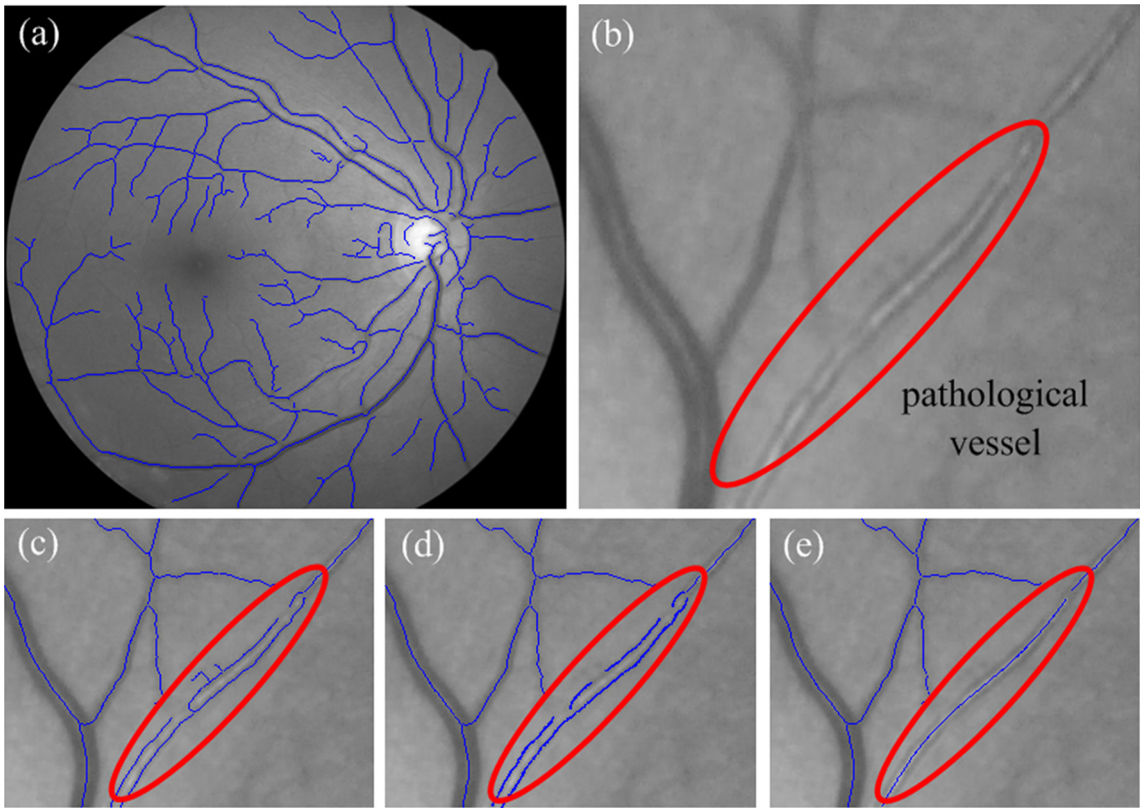

Fig. 4. Example of centerline extraction and correction: (a) extracted vessel centerlines for the retinal image Fig. 3(a); (b) image of a pathological vessel with strong light reflex; (c) extracted centerlines of the pathological vessel; (d) detected wrong centerlines by the parallel line model; (e) corrected centerline of the pathological vessel.

corresponding intensity profiles for a normal vessel and a pathological vessel with central light reflex.

To facilitate the vessel boundary detection in the next step, the axis should be longer enough to cover both the vessel pixels and the background pixels. In the present work, the length l of the measuring axis is set to be $l = 1.6 \times d$, where d is the mean width of the corresponding vessel segment in Section 2.1 obtained by use of the distance transform [29].

2.4. Vessel boundary detection using K-means clustering and boundary searching strategy

The measurement of vascular width requires the detection of vessel boundary. With the intensity profiles along the measuring axis, pixels of vessels and background could be separated based on their difference in intensity level. The outermost vascular pixels could be further identified as vessel boundary.

The unsupervised k-means clustering method [30] is employed in the present work to classify the pixels on the measuring axis. For a given set of n points $(I_1,I_2,I_j,\ldots,I_n)$, the basic idea of k-means is to partition the n points into k clusters $(C_1,C_2,\ldots,C_k)$ with corresponding cluster centers $(c_1,c_2,\ldots,c_k)$ by minimizing the sum of the Euclidean distance of all n points to their corresponding center

$$\arg \min_{(C_1,\ldots,C_k),(c_1,\ldots,c_k)} \sum_{i=1}^{k} \sum_{I_j \in C_i} ||I_j - c_i||^2 \tag{5}$$

For the case where I_j is the intensity value of the j_{th} pixel on the measuring axis, I_j could be classified as 'vessel' (C_1) or 'background' (C_2) by use of Eq. (6), where the threshold value c^* is the average value of the two cluster centers c_1 andc_2.

$$\begin{cases} I_j \in C_1 & \text{if } I_j < c^* \\ I_j \in C_2 & \text{other cases} \end{cases} \tag{6}$$

The clustering result is shown in Fig. 7 for example, where the pixels along measuring axis are labeled either as "vessel" (green colored) or as "background" (red colored). The centerline pixel (O) with intensity of I_m is additionally marked in the figure. It can be seen that, for normal vessels (Fig. 7(a and b)), the pixels on the measuring axis are well classified with the threshold value c^*. For the pathological vessels (Fig. 7(c and d)), however, some vessel pixels near the centerline are incorrectly classified as "background" due to their higher intensities in the light reflex region.

Coping with the various clustering results mentioned above, vessel boundaries can be determined by use of the boundary searching strategy as follows: (i) pixels are scanned from two ends of the measuring axis towards the centerline pixel (the m_{th} pixel); (ii) for pixels at one side of the centerline (at left side when $j + 1 < m$ and right side when $j > m$), pairs of adjacent pixels are first located by use of Eq. (7), followed by averaging coordinates of each pair of adjacent pixels as boundary candidates; finally, (iii) selecting the candidate which is closest to the centerline pixel as the left or right boundary (yellow colored in Fig. 7). After the detection of vessel boundaries, the vessel width can be easily calculated as the Euclidean distance of the two boundary points.

$$\begin{cases} I_j > c^* \text{ and } I_{j+1} < c^* & \text{if } j+1 < m \\ I_j < c^* \text{ and } I_{j+1} > c^* & \text{if } j > m \end{cases} \tag{7}$$

In the following sections, the proposed method will be tested both on the public database REVIEW and on our own dataset, and compared with the state-of-the-art technique. Among recent studies on measurement of vessel width, the ARIA method [20] outperforms other main methods in overall measuring accuracy, and is therefore deemed as the state-of-the-art work.

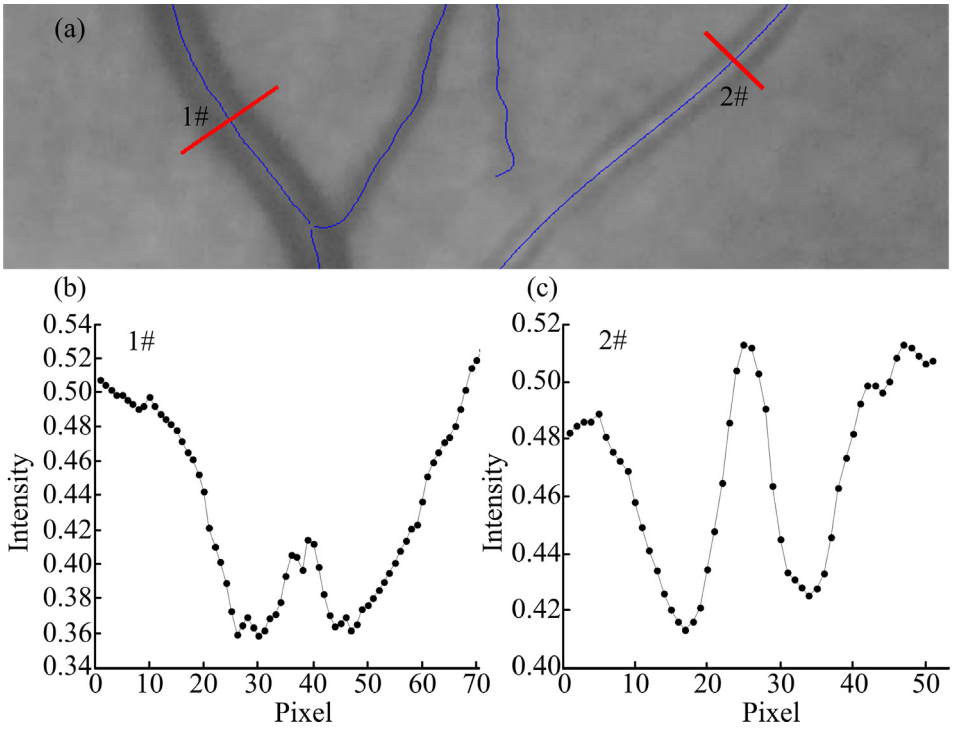

Fig. 6. Example of intensity profiles along the measuring axis: (a) generated measuring axis over a normal vessel (1#) and a pathological vessel with central light reflex (2#); (b) intensity profile on axis 1#; (c) intensity profile on axis 2#.

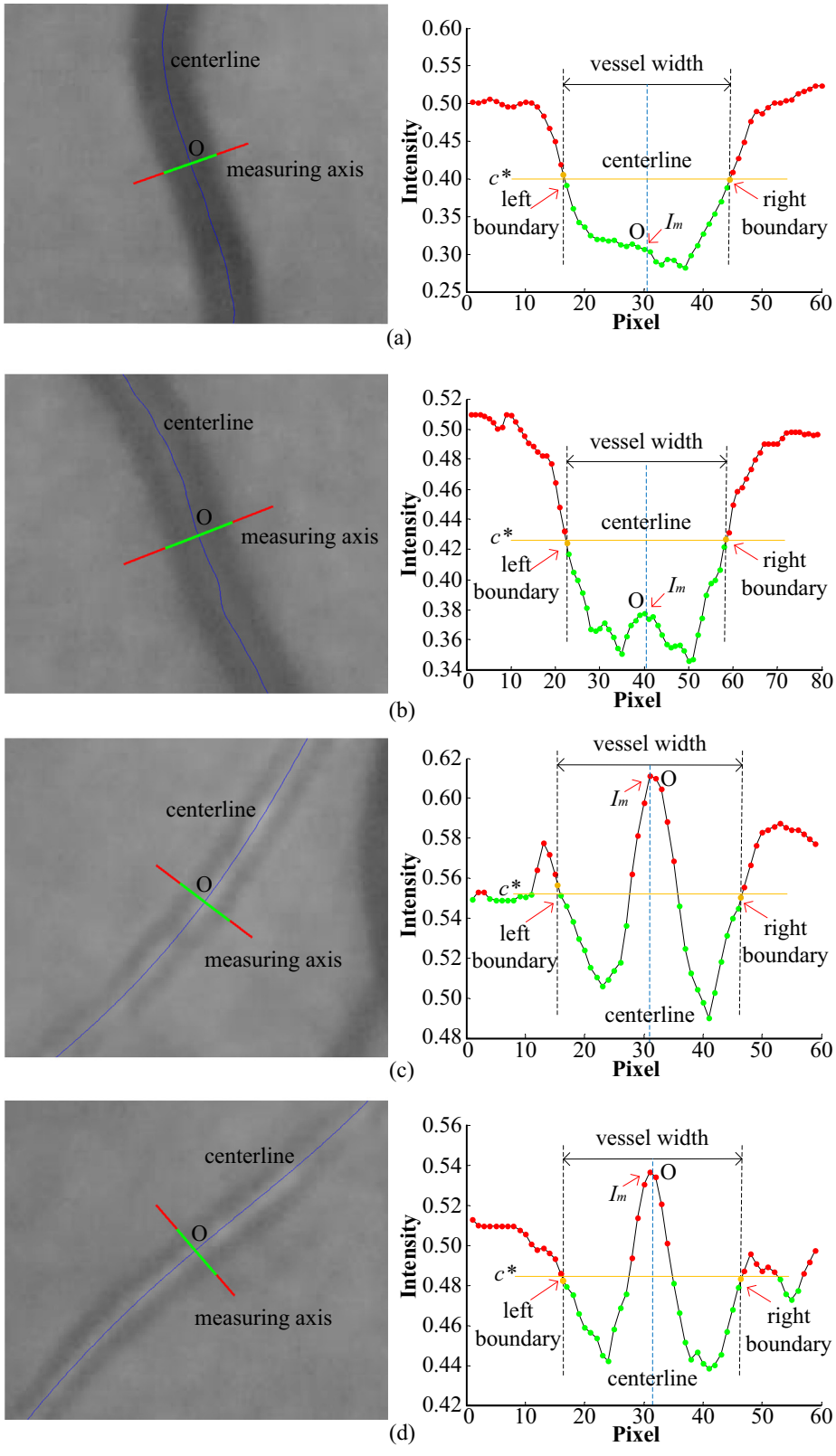

Fig. 7. Vessel boundary detection by *k*-means clustering algorithm and boundary searching strategy: (a) and (b) normal vessels; (c) and (d) pathological vessels.

3. Database and results

3.1. Database

The REVIEW database [26] includes four different image datasets (HRIS, CLRIS, VDIS and KPIS) with varied image size from 1024 × 1360 to 2438 × 3584 pixels, and most vessels in the image have no obvious central light reflex. The REVIEW database also provides marked vessel boundaries and vessel width measured manually by three independent experts (or observers). The ground truth of the vessel width was considered as the mean of the three manual measurements. However, the ground truth is only

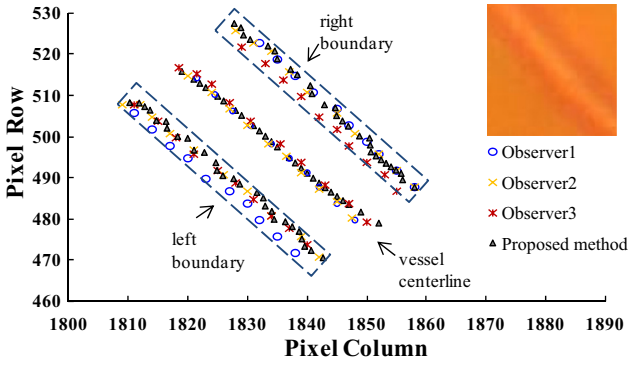

Fig. 8. The boundary and centerline of a vessel obtained by the proposed method and three independent observers.

available for some vessel segments, not for all vessels in the images. In the present work, 22 randomly selected vessel segments (S1#-S22#) from the REVIEW database were used to test the proposed method, involving 700 measured values of vessel width.

To test our proposed measuring method for vessels with central light reflex, retinal images were sampled from a local hospital (Second Xiangya Hospital of Central South University) to constitute our own dataset. The images were captured by the confocal scanning laser ophthalmoscope system HRA2 with a resolution of 2550 × 3050. In the present work, 20 example vessel segments (M1#-M20#, including 15 vessel segments with light reflex, 5 normal vessel segments without light reflex; 270 measured values of vessel width in total) were employed to test the proposed method. The ground truth of vessel boundary and vessel width is taken as the average of manual measurements from three trained experts.

3.2. Results

The profiles of the centerline and boundaries of a vessel detected by the proposed method are shown in Fig. 8 for example, and compared with manual measurement by three independent observers. The measured widths of vessel segment S1#-S22# and M1#-M20 by our proposed method, ARIA method and three observers (ground truth) are compared in Table 1 and Fig. 9. In the table, the measured value is represented in the form of mean and standard deviation, as was also done in [31]. The detected centerline and boundaries of some representative vessel segments (such as healthy vessels at branching and crossing point, pathological vessels with central light reflex) are given in Fig. 10.

Table 1
Measured width of vessel segments from REVIEW dataset and our own dataset.

Data source	Vessel segment	Observer1	Observer2	Observer3	Ground truth	ARIA [20] method	Our method
REVIEW database	S1#	6.35 ± 0.41	7.07 ± 0.46	7.35 ± 0.42	6.93 ± 0.38	5.94 ± 0.47	6.13 ± 0.50
	S2#	7.12 ± 0.51	7.70 ± 0.34	8.05 ± 0.33	7.63 ± 0.33	6.20 ± 0.22	6.25 ± 0.32
	S3#	7.12 ± 0.33	7.71 ± 0.30	8.17 ± 0.44	7.67 ± 0.28	6.64 ± 0.25	6.68 ± 0.35
	S4#	14.80 ± 0.43	15.98 ± 0.50	18.12 ± 0.16	16.30 ± 0.27	15.49 ± 0.14	16.81 ± 0.69
	S5#	15.15 ± 0.55	16.34 ± 0.28	16.88 ± 0.41	16.12 ± 0.36	15.78 ± 0.94	16.66 ± 0.51
	S6#	13.68 ± 1.06	13.69 ± 1.04	16.07 ± 0.50	14.48 ± 0.77	13.08 ± 0.98	14.10 ± 0.61
	S7#	23.03 ± 0.85	23.88 ± 1.20	23.44 ± 2.57	23.45 ± 1.22	22.65 ± 0.62	23.44 ± 0.48
	S8#	17.20 ± 1.61	18.48 ± 1.81	20.14 ± 0.64	18.61 ± 1.30	17.64 ± 1.30	19.12 ± 1.05
	S9#	19.84 ± 0.73	22.52 ± 1.43	19.60 ± 1.00	20.65 ± 0.91	20.90 ± 0.67	21.51 ± 0.83
	S10#	14.86 ± 0.79	15.58 ± 1.73	14.67 ± 1.30	15.04 ± 1.19	14.74 ± 0.96	14.81 ± 0.99
	S11#	11.72 ± 0.96	13.09 ± 1.31	12.35 ± 0.99	12.39 ± 1.03	12.03 ± 0.71	12.55 ± 0.51
	S12#	9.91 ± 1.77	10.45 ± 1.94	10.41 ± 1.38	10.26 ± 1.65	9.81 ± 1.45	10.25 ± 1.00
	S13#	15.05 ± 2.52	15.91 ± 2.21	15.58 ± 1.87	15.51 ± 2.14	15.18 ± 2.28	15.41 ± 1.92
	S14#	11.78 ± 0.85	14.90 ± 1.19	13.00 ± 1.18	13.24 ± 0.58	13.08 ± 1.02	13.75 ± 0.66
	S15#	12.26 ± 0.83	12.60 ± 0.67	13.40 ± 0.87	12.74 ± 0.62	12.31 ± 0.76	12.86 ± 0.67
	S16#	9.61 ± 0.49	11.70 ± 0.68	10.40 ± 0.97	10.58 ± 0.58	9.83 ± 0.50	10.72 ± 0.26
	S17#	20.68 ± 0.35	20.50 ± 0.91	21.20 ± 0.34	20.82 ± 0.40	20.76 ± 0.21	20.95 ± 0.25
	S18#	19.35 ± 0.43	19.30 ± 0.33	20.70 ± 0.45	19.78 ± 0.20	19.96 ± 0.27	20.30 ± 0.56
	S19#	15.95 ± 0.40	16.20 ± 0.43	17.50 ± 0.35	16.54 ± 0.32	16.41 ± 0.48	16.68 ± 0.72
	S20#	25.12 ± 1.32	28.20 ± 0.87	27.40 ± 0.68	26.91 ± 0.79	26.48 ± 1.34	26.31 ± 1.09
	S21#	25.86 ± 1.31	26.60 ± 1.27	28.50 ± 0.65	26.98 ± 0.89	27.43 ± 1.57	27.72 ± 1.24
	S22#	14.75 ± 0.95	16.00 ± 0.57	15.20 ± 0.56	15.33 ± 0.61	14.94 ± 0.57	15.52 ± 0.68
Own dataset	M1#*	26.27 ± 0.91	24.10 ± 1.18	21.57 ± 1.15	23.98 ± 2.22	\	23.64 ± 1.22
	M2#*	34.95 ± 0.34	35.29 ± 0.39	33.24 ± 0.00	34.59 ± 0.93	\	34.60 ± 1.40
	M3#	33.82 ± 0.85	33.75 ± 1.21	32.72 ± 0.34	33.44 ± 0.99	34.43 ± 0.37	33.00 ± 0.63
	M4#	15.26 ± 0.74	14.63 ± 0.95	14.00 ± 0.51	14.63 ± 0.89	14.77 ± 0.26	14.47 ± 0.64
	M5#*	27.91 ± 1.58	27.66 ± 1.49	26.30 ± 0.59	27.29 ± 1.46	\	27.33 ± 1.23
	M6#*	37.47 ± 0.93	37.24 ± 0.60	36.45 ± 0.84	37.05 ± 0.90	\	36.70 ± 1.17
	M7#*	28.92 ± 1.72	28.00 ± 1.65	27.92 ± 1.18	28.20 ± 1.51	\	28.50 ± 1.29
	M8#*	30.29 ± 1.04	30.10 ± 0.76	30.19 ± 0.52	30.20 ± 0.79	\	29.40 ± 1.40
	M9#*	24.44 ± 0.86	24.04 ± 1.74	22.44 ± 0.55	23.64 ± 1.43	\	23.55 ± 0.82
	M10#*	26.74 ± 1.04	27.11 ± 1.59	27.21 ± 0.55	27.02 ± 1.12	\	27.60 ± 1.35
	M11#*	25.04 ± 0.76	24.07 ± 0.91	22.75 ± 0.59	23.96 ± 1.21	\	24.08 ± 0.67
	M12#*	24.82 ± 0.95	25.50 ± 1.81	23.21 ± 1.01	24.51 ± 1.60	\	25.45 ± 1.29
	M13#*	36.89 ± 0.42	36.30 ± 1.65	36.05 ± 0.51	36.42 ± 1.02	\	36.67 ± 0.82
	M14#*	38.29 ± 0.98	37.80 ± 0.62	38.63 ± 0.34	38.24 ± 0.74	\	38.29 ± 0.76
	M15#	29.98 ± 0.76	29.49 ± 3.00	30.00 ± 0.00	29.83 ± 1.68	29.42 ± 0.42	30.91 ± 0.70
	M16#	43.55 ± 0.94	43.56 ± 1.15	45.21 ± 0.35	44.11 ± 1.17	44.61 ± 0.19	44.00 ± 0.73
	M17#	43.67 ± 0.90	43.80 ± 0.56	43.12 ± 0.33	43.58 ± 0.71	43.69 ± 0.50	43.31 ± 0.70
	M18#*	21.22 ± 0.95	23.17 ± 1.23	23.97 ± 0.63	22.79 ± 1.50	22.55 ± 0.92	22.00 ± 1.10
	M19#*	19.72 ± 0.27	20.14 ± 0.56	21.33 ± 0.49	20.40 ± 0.82	19.53 ± 0.18	20.00 ± 0.00
	M20#*	24.64 ± 1.34	24.76 ± 0.86	22.70 ± 0.23	24.03 ± 1.32	24.33 ± 0.66	24.91 ± 0.94

Note: the symbol * represents that it is a pathological vessel segment; \ means that ARIA method is not valid in that case.

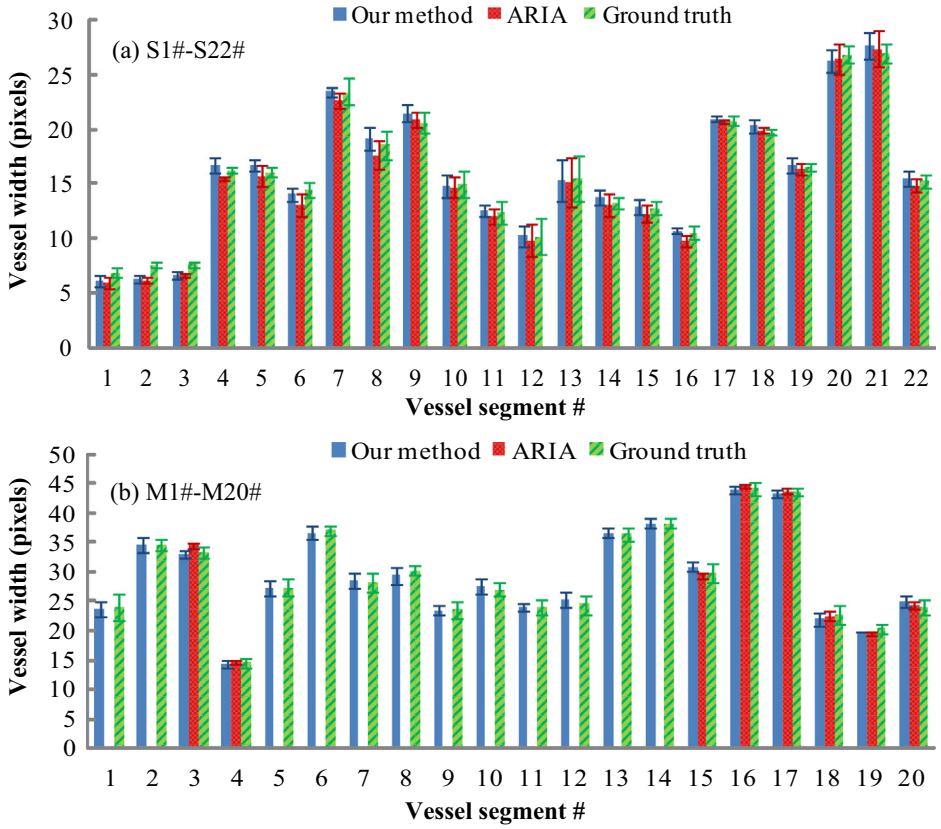

Fig. 9. Comparison of vessel width measured by the proposed method, ARIA method and the ground truth. The testing vessel segments are (a) S1#-S22# from REVIEW and (b) M1#-M20# from our own dataset.

The obtained centerline map and width map for a complete retinal image are shown in Fig. 11 for example. In comparison, the ARIA method and the proposed method employ the same image processing procedures to extract the vessel tree from the raw image.

4. Discussion

4.1. Accuracy and advantages of the proposed method

When comparing the vessel centerline and vessel boundaries detected by our proposed method with those labeled by three independent observers (see Fig. 8), we could say that the proposed method has satisfactory accuracy, considering the fact that there exist also deviations between manual measurements by the three observers. For further comparison, the mean of the three manual measurements are taken as ground truth.

The test results on REVIEW dataset (see S1#-S22# in Table 1 and Fig. 9(a)) demonstrate that both our method and the ARIA method [20] agree very well with ground truth for the 20 vessel segments (S1#, S4#-S22#). The worst performance of our method occurs at vessel segment S2# with relative error of 18%. In contrast, the worst performance of ARIA happens at S2# with relative error of 19%.

Although our proposed method has comparable accuracy in measuring the width of normal vessels (vessels that have no obvious central light reflex), it is more advantageous in measuring pathological vessels with central light reflex. As demonstrated by the test on 15 pathological vessels from our own dataset (Table 1 and Fig. 9(b)), ARIA method is capable of measuring 20% of them (three segments: M18#-M20#), but fails in measuring the other 12 pathological vessel segments. In contrast, our proposed method is able to measure all the 15 pathological vessel segments with negligibly small deviation from the ground truth. As can be seen from Fig. 10, the vessel width of healthy vessels (Fig. 10(c and d)) generated by ARIA method and the proposed method is correct in general. For pathological vessel with central light reflex (Fig. 10 (a and b)), however, the ARIA method recognizes it as two separated vessels with two separated centerlines, leading to false results in the width map.

For all the 42 testing vessel segments (normal vessels and pathological vessels) shown in Table 1, the ARIA method is capable of measuring 71% of them, with an average measuring error of 4%. In contrast, the proposed method succeeds in measuring all of them with an average measuring error of 3%. In other words, the proposed method has comparable measuring accuracy to ARIA method, but it is more advantageous in measuring pathological vessels with central light reflex.

A retinal image contains many vessels that may have different morphologies or illumination conditions. It is thus necessary to test the effectiveness of our proposed measuring method on the whole image. Fig. 11 gives the measuring results of the entire vessel tree. Vessel *A, B, E* in Fig. 11 are pathological. Because of the central light reflex within these vessel segments, the vessels become separated (Fig. 11(b)) in the procedure of vessel segmentation. By use of the parallel line model proposed in the present work, the centerlines of the separated segmented vessels can be detected and corrected (see vessel *A, B, E* in Fig. 11(c)), based on which the vessel boundary and vessel width is correctly determined using *k*-means clustering algorithm and the boundary searching strategy (see Fig. 11(d)).

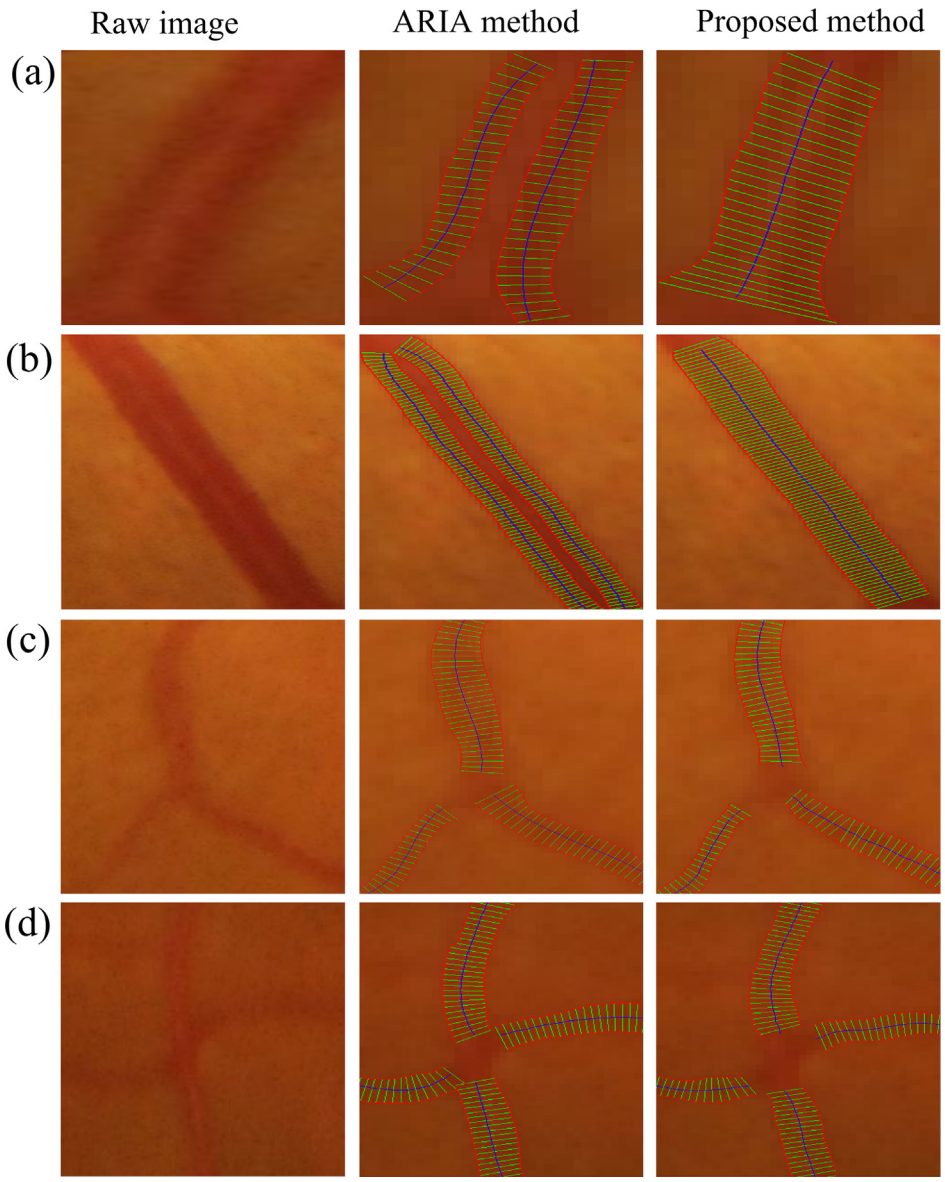

Fig. 10. Comparison of measuring results between ARIA method and the proposed method. (a and b) are pathological vessels; (c and d) are healthy vessels. The detected centerline (marked blue), boundary (red) and width (green) are presented. (For interpretation of the references to colour in this figure legend, the reader is referred to the web version of this article.)

4.2. Justification of using IUWT in segmentation procedure of our method

In our method, vessel segmentation is one primary procedure for it effects the measuring results by directly effecting the procedure of extraction and refinement of centerline. Even the measuring results mentioned above already verified the effectiveness and advantages of our method (average relative error: 3% vs. 4%), it is still necessary to figure out the justification of using IUWT method in the vessel segmentation procedure.

In Table 2, we compare IUWT method with 8 recent segmentation methods in the aspects of segmentation accuracy and processing time on 20 test images of public DRIVE database (manual segmentations are provided in this database). The adopted measure for segmentation evaluation is accuracy (calculated as the proportion of correctly classified pixels). It is demonstrated that compared with manual segmentation accuracy of 0.9473, all the recent methods show good performance (accuracy >0.93). The supervised method provided in reference [38] has the highest accuracy of 0.9466, but it needs 9 h for training segmentation model and it costs 180 s to process each image. IUWT shows comparable good accuracy of 0.9371. Although IUWT does not have the highest segmentation accuracy, it has significant advantage in aspects of processing time (only 0.041 s for each image). Moreover, IUWT belongs to unsupervised method and no training time is needed. It is thus reasonable to use IUWT for segmentation in our method.

4.3. Limitation of the proposed measuring method

Even it is justified that the employed IUWT segmentation method has good performance, similar to other methods for vessel width measurement [17,18,20], the measuring errors of our method brought by wrong/missed segmentation cannot be totally avoided either. When observing the width map obtained by the proposed method, we can find that there are still some vessels that

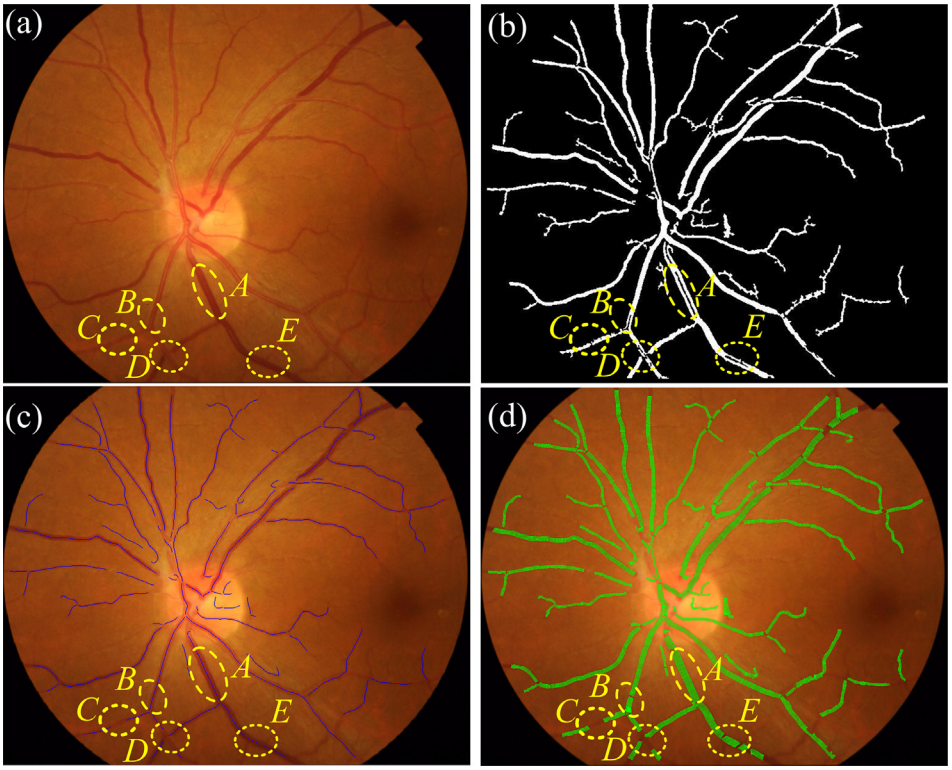

Fig. 11. Example of measuring results by the proposed method: (a) raw image; (b) segmented vessels; (c) centerline maps (blue colored); (d) width maps (green colored). (For interpretation of the references to colour in this figure legend, the reader is referred to the web version of this article.)

Table 2
Performance comparison of IUWT and other recent segmentation methods on DRIVE dataset.

Method	Processor	RAM	Average accuracy	Average processing time
Manual (second observer)	––	––	0.9473	7200 s
Unsupervised methods				
IUWT	3.3 GHz	8 GB	0.9371	0.041 s
Nguyen et al. [32]	3.3 GHz	8 GB	0.9407	0.924 s
José Ignacio et al. [33]	––	––	0.9437	––
Dai, Luo et al. [34]	3.3 GHz	8 GB	0.9364	109.446 s
Supervised methods				
Joes et al. [35]	1.0 GHz	1 GB	0.9441	900 s
Strisciuglio et al. [36]	1.8 GHz	4 GB	0.9454	75 s
Al-Rawi et al. [37]	1.7 GHz	––	0.9420	2.156 s
Soares et al. [38]	2.1 GHz	1 GB	0.9466	180 s (9 h for training)
Orlando et al. [39]	2.9 GHz	64 GB	0.9454	1 s (training time not provided))

The processing time of IUWT and methods in references [32–34] are obtained by our own computing platform. The processing time of the other methods [35–39] are reported in the corresponding original papers.

cannot be measured, such as vessels in the marked regions *C* and *D* in Fig. 11(c) and (d). This is because vessel pixels that have similar intensities to background (for example region *D*) cannot be segmented; or the segmented vessels (for example regions *C*) contain spurs after morphological thinning, which are recognized as short segments and are thus discarded [20].

The aforementioned measuring errors brought by wrong/missed segmentations could be possibly reduced by choosing more accurate (usually also complex) vessel segmentation algorithms. However, the corresponding improvements on measuring accuracy maybe limited. This is for the accuracy of the employed IUWT is already high (accuracy of 0.9371) among recent segmentation methods, only a small increase of segmentation accuracy over IUWT method can be achieved. The time cost for measuring the vessel width will also be greatly increased if a more accurate (usually needs more training time/processing time) vessel segmentation method is employed.

5. Conclusion

Sustained change in the width of retinal vessel may be related with retinopathy or diseases in circulatory system. It is thus meaningful to measure the vessel width for quantitative diagnosis. However, some vessels (especially pathological vessels) often show central light reflex in retinal images, resulting in failures or errors in the measurement of the vessel width.

Based on the state-of-the-art technique (ARIA method) [20], the present work contributes to provide an improved method for measuring vessel width in retinal image. With it, pathological vessels with central light reflex can be measured by using a parallel line model and *k*-means clustering algorithm.

The proposed measuring method was tested on vessel segments and on whole retinal image, using the public database REVIEW and our own dataset containing more pathological vessels. The measuring results were also compared with ARIA method. It can be concluded that: (i) the proposed parallel line model is effective in extracting the centerline of pathological vessels with central light reflex; (ii) by use of *k*-means clustering algorithm and the boundary searching strategy, the vessel boundary on the measuring axis can be identified; (iii) the proposed method is capable of measuring both normal vessels and pathological vessels. Comparisons demonstrate that it has comparable measuring accuracy to ARIA method (relative measuring error: 3% vs. 4%), but is more advantageous in measuring pathological vessels with central light reflex. It succeeds in measuring all the testing pathological vessels whereas ARIA is capable of measuring 20% of them.

Nevertheless, the proposed method (and the ARIA method) has limitation in generating a complete width map for all vessels in the image. A possible solution is to choose more accurate (usually also complex) image segmentation algorithms. However, the total computing time could be greatly increased.

Acknowledgments

This work is supported by Hunan Key Laboratory of Intelligent Robot Technology in Electronic Manufacturing (IRT2018001). The authors would like to thank Peter Bankhead for providing the ARIA software (https://doi.org/10.1371/journal.pone.0032435.s001). The editors and the reviewers are also appreciated for their suggestions greatly improved this paper.

Conflict of interest

The authors have no relevant financial interests and no potential conflicts of interest in the manuscript.

References

[1] A. Bhuiyan, B. Nath, J.J. Chua, K. Ramamohanarao, An efficient method for vessel width measurement on color retinal images Funchal, Madeira, Portugal, in: International Conference on Biomedical Electronics and Devices, Biosignals 2008, 2015, pp. 178–185.
[2] K. Jew, U.R. Acharya, Y. Hagiwara, U. Raghavendra, J.H. Tan, S.V. Sree, S.V. Bhandary, A.K. Rao, S. Sivaprasad, K.C. Chua, Diagnosis of retinal health in digital fundus images using continuous wavelet transform (CWT) and entropies, Comput. Biol. Med. 84 (2017) 89–97.
[3] Y. Guo, Ü. Budak, L.J. Vespa, E. Khorasani, A. Şengür, A retinal vessel detection approach using convolution neural network with reinforcement sample learning strategy, Measurement 125 (2018) 586–591.
[4] M.D. Knudtson, B.E.K. Klein, R. Klein, T.Y. Wong, L.D. Hubbard, K.E. Lee, S.M. Meuer, C.P. Bulla, Variation associated with measurement of retinal vessel diameters at different points in the pulse cycle, Br. J. Ophthalmol. 88 (2004) 57–61.
[5] M.E. Gegundez-Arias, D. Marin, B. Ponte, F. Alvarez, J. Garrido, C. Ortega, M.J. Vasallo, J.M. Bravo, A tool for automated diabetic retinopathy pre-screening based on retinal image computer analysis, Comput. Biol. Med. 88 (2017) 100–109.
[6] S.S. Kar, S.P. Maity, Retinal blood vessel extraction using tunable bandpass filter and fuzzy conditional entropy, Comput. Methods Programs Biomed. 133 (2016) 111–132.
[7] M.M. Fraz, S.A. Barman, P. Remagnino, A. Hoppe, A. Basit, B. Uyyanonvara, A.R. Rudnicka, C.G. Owen, An approach to localize the retinal blood vessels using bit planes and centerline detection, Comput. Methods Programs Biomed. 108 (2012) 600–616.
[8] G. Stabingis, J. Bernatavičienė, G. Dzemyda, A. Paunksnis, P. Treigys, R. Vaičaitienė, L. Stabingienė, Automatization of eye fundus vessel width measurements, Eur. Congr. Comput. Methods Appl. Sci. Eng. (2017) 787–796.
[9] S. Goswami, S. Goswami, S. De, Automatic Measurement and Analysis of Vessel Width in Retinal Fundus Image, Springer, Singapore, 2017.
[10] https://meyerinst.com/library/Image-Pro_Plus_Life_Science_Brochure_Catalog.pdf. (accessed 27.09.2018).
[11] F. Huang, B. Dashtbozorg, A.K.S. Yeung, J. Zhang, T.T.J.M. Berendschot, B.M.T.H. Romeny, A Comparative Study Towards the Establishment of an Automatic Retinal Vessel Width Measurement Technique, (2017) 227-234.
[12] O.H. Brinchmann-Hansen, Halvor Heier, Theoretical relations between light streak characteristics and optical properties of retinal vessels, Acta Ophthalmol. 64 (1986) 33–37.
[13] P.H. Gregson, Z. Shen, R.C. Scott, V. Kozousek, Automated grading of venous beading, Comput. Biomed. Res. Int. J. 28 (1995) 291–304.
[14] L. Zhou, M.S. Rzeszotarski, L.J. Singerman, J.M. Chokreff, The detection and quantification of retinopathy using digital angiograms, IEEE Trans. Med. Imaging 13 (1994) 619–626.
[15] J. Lowell, A. Hunter, D. Steel, A. Basu, R. Ryder, R.L. Kennedy, Measurement of retinal vessel widths from fundus images based on 2-D modeling, Med. Imaging IEEE Trans. 23 (2004) 1196–1204.
[16] H. Li, W. Hsu, M.L. Lee, H. Wang, A piecewise Gaussian model for profiling and differentiating retinal vessels, in: International Conference on Image Processing, 2003. ICIP 2003. Proceedings, 2003, pp. 1069–1072.
[17] B. Al-Diri, A. Hunter, D. Steel, An active contour model for segmenting and measuring retinal vessels, IEEE Trans. Med. Imaging 28 (2009) 1488.
[18] X. Xu, M. Niemeijer, Q. Song, M. Sonka, M.K. Garvin, J.M. Reinhardt, M.D. Abràmoff, Vessel boundary delineation on fundus images using graph-based approach, IEEE Trans. Med. Imaging 30 (2011) 1184–1191.
[19] C.A. Lupaşcu, D. Tegolo, E. Trucco, Accurate estimation of retinal vessel width using bagged decision trees and an extended multiresolution Hermite model, Med. Image Anal. 17 (2013) 1164–1180.
[20] P. Bankhead, C.N. Scholfield, J.G. Mcgeown, T.M. Curtis, Fast retinal vessel detection and measurement using wavelets and edge location refinement, PLoS One 7 (2012) e32435.
[21] D.K. Kumar, B. Aliahmad, H. Hao, Retinal vessel diameter measurement using unsupervised linear discriminant analysis, Isrn Ophthalmol 2012 (2012) 151369.
[22] O. Brinchmann-Hansen, H. Heier, The apparent and true width of the blood column in retinal vessels, Acta Ophthalmol. 64 (2010) 29–32.
[23] M.D. Olaf Brinchmann-Hansen, C.C. Christensen, K. Myhre, The response of the light reflex of retinal vessels to reduced blood pressure in hypertensive patients, Acta Ophthalmol. 68 (2010) 155–161.
[24] S. Kaushik, A.G. Tan, P. Mitchell, J.J. Wang, Prevalence and associations of enhanced retinal arteriolar light reflex: a new look at an old sign, Ophthalmology 114 (2007) 113–120.
[25] A. Bhuiyan, C.Y. Cheung, S. Frost, E.L. Lamoureux, P. Mitchell, Y. Kanagasingam, T.Y. Wong, Development and reliability of retinal arteriolar central light reflex quantification system: a new approach for severity grading, Invest. Ophthalmol. Vis. Sci. 55 (2014) 7975–7981.
[26] B. Al-Diri, A. Hunter, D. Steel, M. Habib, REVIEW – a reference data set for retinal vessel profiles, Int. Conf. IEEE Eng. Med. Biol. Soc. 2008 (2008) 2262–2265.
[27] A. Fathi, A.R. Naghsh-Nilchi, Automatic wavelet-based retinal blood vessels segmentation and vessel diameter estimation, Biomed. Signal Process. Control 8 (2013) 71–80.
[28] H.N. Nguyen, T.Y. Kam, P.Y. Cheng, A novel automatic concrete surface crack identification using isotropic undecimated wavelet transform, in: International Symposium on Intelligent Signal Processing and Communications Systems, 2013, pp. 766–771.
[29] R. Fabbri, L.D.F. Costa, J.C. Torelli, O.M. Bruno, 2D Euclidean distance transform algorithms: a comparative survey, ACM Comput. Surv. 40 (2008) 1–44.
[30] H.M. Liu, J.G. Lu, Brief survey of K-means clustering algorithms, Appl. Mech. Mater. 740 (2015) 624–628.
[31] J. Zhang, H. Li, Q. Nie, L. Cheng, A retinal vessel boundary tracking method based on Bayesian theory and multi-scale line detection, Comput. Med. Imaging Graph. 38 (2014) 517–525.
[32] U.T.V. Nguyen, A. Bhuiyan, L.A.F. Park, K. Ramamohanarao, An effective retinal blood vessel segmentation method using multi-scale line detection, Pattern Recognit. 46 (2013) 703–715.
[33] O. José Ignacio, B. Matthew, Learning fully-connected CRFs for blood vessel segmentation in retinal images, in: International Conference on Medical Image Computing & Computer-assisted Intervention, 2014, pp. 634–641.
[34] P. Dai, H. Luo, H. Sheng, Y. Zhao, L. Li, J. Wu, Y. Zhao, K. Suzuki, A new approach to segment both main and peripheral retinal vessels based on gray-voting and gaussian mixture model, PLoS One 10 (2015) e0127748.
[35] S. Joes, M.D. Abràmoff, N. Meindert, M.A. Viergever, V.G. Bram, Ridge-based vessel segmentation in color images of the retina, IEEE Trans. Med. Imaging 23 (2004) 501–509.
[36] N. Strisciuglio, G. Azzopardi, M. Vento, N. Petkov, Supervised vessel delineation in retinal fundus images with the automatic selection of B -COSFIRE filters, Mach. Vis. Appl. 27 (2016) 1137–1149.
[37] M. Al-Rawi, H. Karajeh, Genetic algorithm matched filter optimization for automated detection of blood vessels from digital retinal images, Comput. Methods Programs Biomed. 87 (2007) 248–253.
[38] J.O.V.B. Soares, J.J.G. Leandro, R.M. Cesar Jr., H.F. Jelinek, M.J. Cree, Retinal vessel segmentation using the 2-D Gabor wavelet and supervised classification, IEEE Trans. Med. Imaging 25 (2006) 1214–1222.
[39] J. Orlando, E. Prokofyeva, M. Blaschko, A discriminatively trained fully connected conditional random field model for blood vessel segmentation in fundus images, IEEE Trans. Bio-med. Eng. 64 (2016) 16–27.